The discrepancy in the Cauchy relations is given by

$$C_{12}-C_{44}=\gamma-(16/3)\beta, \quad \text{for bcc}$$
$$=\gamma-8\beta, \quad \text{for fcc.}$$

Thus, not only does our model take into account the effect of the free electrons on the Cauchy relations but it also provides for the modification of internal equilibrium due to the electron gas. In fact, without free electrons we must have $\beta=\partial W/\partial r$ (short range)$=0$.

Thus, this result is in agreement with Fuchs's calculations of the Cauchy relations.

We are doing calculations with this model for various metals and the results will be published elsewhere. The results seem to be in good agreement with experiment.

PHYSICAL REVIEW VOLUME 169, NUMBER 3 15 MAY 1968

Photoemission and Optical Studies of the Electronic Structure of Palladium*

A. Y-C. Yu† AND W. E. Spicer
Stanford Electronics Laboratories, Stanford University, Stanford, California
(Received 29 December 1967)

Photoemission and optical-reflectivity measurements have been carried out on palladium samples prepared and measured in vacuum of approximately 5×10^{-9} Torr for $h\nu\leq11.8$ eV. In addition, photoemission measurements were made on Pd samples in poorer vacuum for $h\nu=16.8$ and 21.3 eV. The optical functions ϵ_1, ϵ_2, $\omega\sigma$, α, and $\mathrm{Im}(1/\epsilon)$ have been calculated from reflectivity data by Kramers-Kronig analysis. Optical transitions are found to be predominantly nondirect in the spectral range studied, although relatively weak direct (or nonconstant-matrix-element) transitions are also observed for 11.8 eV$>h\nu>$9.8 eV. The valence-band optical density of states of Pd, deduced from photoemission and reflectivity data, has peaks at $E-E_f=-0.1$ and -1.1 eV and is lacking in strong structure elsewhere. There is no evidence for a high density of states near $E-E_f=-5$ eV as in Ni, Co, Fe, and Cr. The d-band structures in Pd and Ag are found to be related rather well by the rigid-band model. Values for the density of states at the Fermi energy in Pd are obtained, and are found to be in reasonable agreement (within experimental accuracy) with values obtained from band calculations. A strong peak in the loss function obtained from reflectivity data is observed at $h\nu=7.5$ eV. This correlates with the strong peak observed at 6.8 eV in energy-loss measurements and is probably due to plasma resonance. Detailed analysis of the photoemission and optical data indicate that a peak in the energy-distribution curves, which appears 7.5 eV below the maximum energy in the energy distributions for $h\nu=18.6$ and 21.3 eV, is due to electrons scattered by this plasma resonance.

I. INTRODUCTION

FROM photoemission and optical studies it has been possible to obtain the optical density of states of a number of transition and noble metals. The optical densities of states of the $3d$ ferromagnetic metals—Fe,[1] Co,[2] and Ni[3]—all have a strong peak at about 5 eV below the Fermi level. Recent work by Lapeyre[4] indicates a peak in Cr near 5 eV but weaker in intensity than that in the ferromagnetic transition metals. The paramagnetic metal palladium lies directly below Ni in the periodic table and from band theory its electronic structures would be expected to be similar to that of Ni. If the anomalous peak is associated with ferromagnetism in the $3d$ transition metals, it should not appear in Pd.[5] Therefore, experimental data on the electronic structure of Pd over a wide energy range (~10 eV) are of considerable interest. In this paper, photoemission and optical-reflection data on Pd are presented and the optical density of states determined. These results are discussed in terms of its electronic structure. Results on Pt will be presented in subsequent papers.

II. EXPERIMENTAL METHODS

Photoemission and optical-reflectivity measurements were made on Pd samples prepared and kept in a continuously pumped (oil-free, VacIon system) stainless-steel chamber (pressure during measurement was about 5×10^{-9} Torr). Two methods of sample preparation were used: evaporation by e-gun evaporator and heat cleaning in high vacuum. In the e-gun evaporator (manufactured by Varian Associates), the evaporant (99.99% pure, obtained from Electronic Space Products, Los Angeles), placed on a water-cooled crucible, was evaporated by electron-beam bombardment. The

* Work supported by the National Science Foundation and by the Advanced Research Projects Agency through the Center for Materials Research at Stanford University.
† Present address: Fairchild Semiconductor Research and Development Laboratory, Palo Alto, Calif.
[1] A. J. Blodgett, Jr., and W. E. Spicer, Phys. Rev. **158**, 514 (1967).
[2] A. Y-C. Yu, T. M. Donovan, and W. E. Spicer (to be published); A. Y-C. Yu and W. E. Spicer (to be published).
[3] A. J. Blodgett, Jr., and W. E. Spicer, Phys. Rev. **146**, 390 (1966).
[4] G. L. Lapeyre and K. A. Kress, Phys. Rev. **166**, 589 (1968).
[5] A. Y-C. Yu and W. E. Spicer, Phys. Rev. Letters **17**, 1171 (1966).

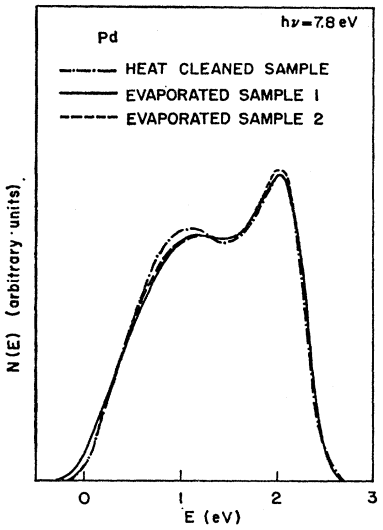

FIG. 1. Photoemitted electron energy distribution curves at $h\nu=7.8$ eV for three different palladium samples.

crucible was cooled sufficiently so that it could not alloy with the evaporant. The pressure during evaporation was about 7×10^{-8} Torr and the time of evaporation was about 5 min. In the heat-cleaning method, a tungsten heater was placed behind a thin (0.025-in.) Pb substrate. Heating the sample to 800°C for 20 h in high vacuum (2×10^{-9} Torr) was sufficient to produce a clean surface suitable for our measurements. Photoemission results from samples formed by these two methods of preparation are reproducible and identical. In Figs. 1 and 2, photoemitted electron energy distribution curves (EDCs) at $h\nu=7.8$ and 10.2 eV of two e-gun evaporated samples and one heat-cleaned sample are compared. It is clear that all three samples show almost exactly the same structure. Samples were also prepared by evaporation from tungsten filaments. Photoemission results of such samples were not reproducible, apparently due to

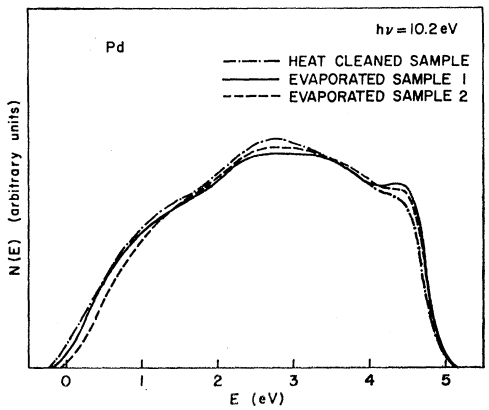

FIG. 2. Photoemitted electron energy distribution curves at $h\nu=10.2$ eV for three different palladium samples.

alloying of W with Pd;[6] therefore, no results obtained from such samples are reported here.

Attempts were made to reduce the work function of Pd by depositing a monolayer of Cs. Unfortunately, Cs appeared to diffuse into, and alloyed with, Pd, so that its electronic structure and thus the photoemission results were changed. Unable to reduce the work function, we tried to extend the measurements to higher photon energies than 11.8 eV, which was the cutoff photon energies of the LiF window used on our vacuum chamber. We constructed a special knockoff tube for this purpose. In this tube, the substrate was heat cleaned in high vacuum ($\sim2\times10^{-9}$ Torr) at 800°C for 20 h. After the heat cleaning, the EDCs of this sample were almost identical to those of high-vacuum e-gun evaporated samples (see Figs. 1 and 2). The unique feature of this tube was that the LiF window was mounted on a thin-wall neck and can be knocked off easily, permitting photoemission measurements made on the sample exposed only to the pressure of the vacuum monochromator ($\sim2\times10^{-5}$ Torr). Results of such low-vacuum samples will be presented in Sec. IV C.

Techniques for making photoemission[7] and optical-reflectivity[2,6] measurements have been reported elsewhere and shall not be discussed here.

III. OPTICAL PROPERTIES OF PALLADIUM

Available optical-reflectivity data on Pd are either taken on samples prepared in poor vacuum[8,9] or incomplete[10] (Ref. 10 does not have data for $h\nu<3.8$ eV). We have measured the near normal-incidence reflectivity of high-vacuum e-gun evaporated Pd samples in the spectral region 2.2 eV$\leq$11.6 eV. The method of sample preparation was that discussed in Sec. II.

Two samples have been studied and their reflectance found to be practically identical. Below $h\nu=2.2$ eV, the reflectance has been extrapolated by the Hagen-Ruben formula.[11] The curve joins smoothly onto the measured one. No adjustable parameter was used. In Fig. 3, the reflectance of Pd so obtained is shown. The reflectance is quite smooth, with slight shoulders at 3 and 6 eV. It is almost a constant for $h\nu>8.5$ eV.

To apply the Kramers-Kronig (KK) analysis, the reflectance curve for $h\nu>11.6$ eV has been extrapolated by an exponential, which was adjusted to have the calculated ϵ_2 agree with that of Robin[10] in the near-uv region. The results of ϵ_1 and ϵ_2 are shown in Fig. 4.

[6] A. Y-C. Yu, Ph.D. thesis, Stanford University, 1967 (unpublished).
[7] W. E. Spicer and C. N. Berglund, Rev. Sci. Instr. 35, 1665 (1964).
[8] G. B. Sabine, Phys. Rev. 55, 1064 (1939).
[9] *Landolt-Börnstein Zahlenwerte und Funktionen* (Springer-Verlag, Berlin, 1967), 8 Teil, pp. 1–8.
[10] S. Robin, in *Optical Properties and Electronic Structure of Metals and Alloys* (North-Holland Publishing Co., Amsterdam, 1966), p. 202.
[11] F. Seitz, *The Modern Theory of Solids* (McGraw-Hill Book Co., New York, 1940).

Our ϵ_2 agrees with that of Robin very well for $h\nu<5.5$ eV. For $h\nu>7.5$ eV, our ϵ_2 lies lower. Since our sample was prepared and measured in ultrahigh vacuum, the lower absorption is probably due to the absence of oxide film on our sample. In Fig. 5, $\omega\sigma$, which gives the total optical transition probability per unit time, is shown. There are broad peaks at $h\nu=2$ and 5 eV and a steep rise starting at about 7.6 eV. Figure 6 shows the absorption coefficient α of Pd. It has structure similar to that in $\omega\sigma$. The origin of this structure will be discussed later.

Figure 7 shows the energy loss function, $-\mathrm{Im}(1/\epsilon)$, of Pd, which has a strong peak at $h\nu=7.5$ eV. At this photon energy, both ϵ_1 and ϵ_2 are small ($\epsilon=0$ at $h\nu=7.3$ eV) and they have positive and negative slopes,

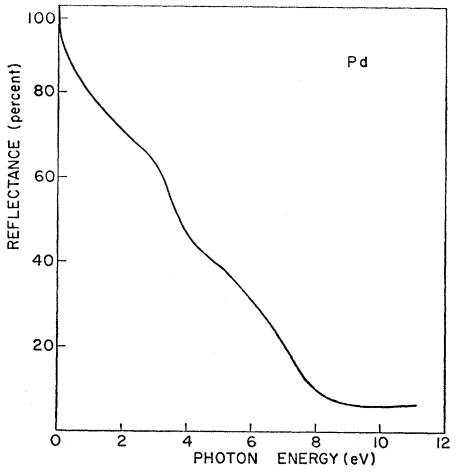

FIG. 3. Reflectance of palladium.

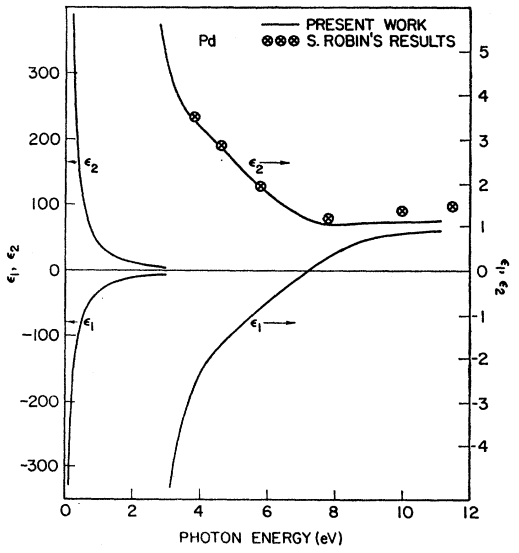

FIG. 4. The real and imaginary parts of the dielectric constant of palladium. The solid curve gives the results obtained in this work. ⊗⊗ indicate the results obtained by S. Robins (Ref. 10).

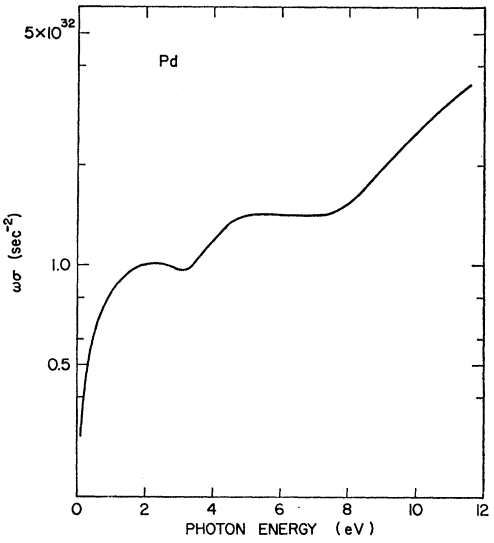

FIG. 5. The optical conductivity times frequency $\omega\sigma$ (ω) for palladium.

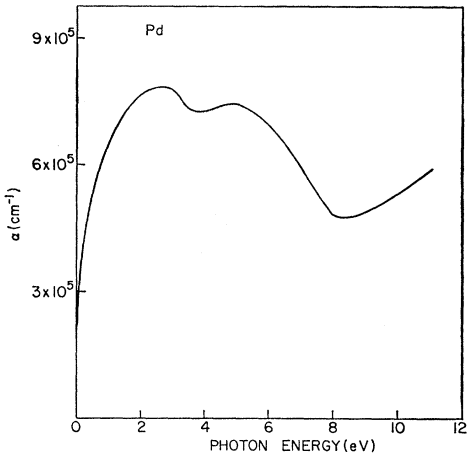

FIG. 6. The absorption coefficient α of palladium.

respectively. This is characteristic of a plasmon resonance.[12] It is interesting to note that a strong peak also occurs in the energy-loss spectrum of Pd (Fig. 8), with primary electron energies at 6.8±0.2 eV.[13] Thus available data indicate that the plasmon energy in Pd could be near 7.5 eV. More discussion of this point will be presented in Sec. VI.

IV. EXPERIMENTAL PHOTOEMISSION RESULTS FROM Pd

A. Quantum Yield of High-Vacuum Samples

The quantum yields of two *e*-gun-evaporated Pd samples are shown in Fig. 9. The yield is very low, rising

[12] H. R. Philipp, in *Optical Properties and Electronic Structure of Metals and Alloys* (North-Holland Publishing Co., Amsterdam, 1966), p. 414.

[13] J. L. Robins, Proc. Phys. Soc. (London) **78**, 1177 (1961).

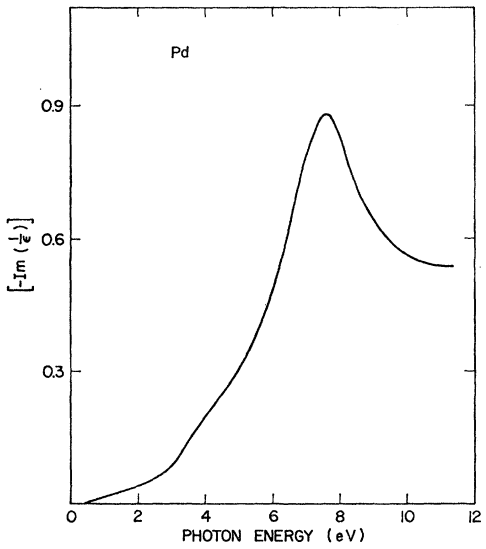

FIG. 7. Plot of energy loss function $[-\mathrm{Im}/(1/\epsilon)]$ of palladium.

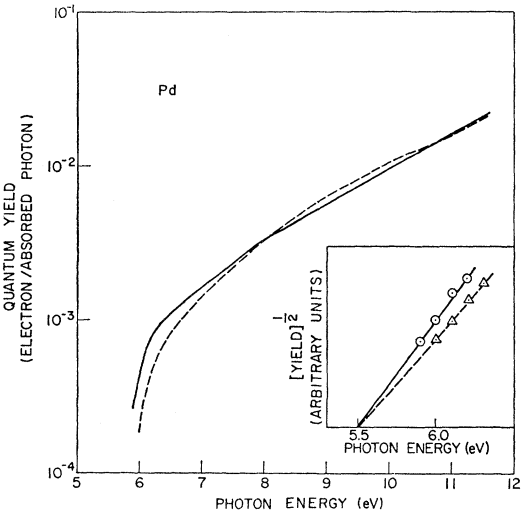

FIG. 9. Specter distribution of the quantum yield from two palladium samples. In the insert the half-power of the yield is plotted versus $h\nu$. A work function of 5.5 eV is obtained from these plots.

to only about 0.02 electron per absorbed photon at $h\nu=11.5$ eV. The yield curve is smoother and lacking of strong structure. By the Fowler method,[14] the work function of these Pd samples was determined to be 5.5 eV, in reasonable agreement with the value (5.4 eV) compiled by Suhrmann and Wedler[15] on crystallographically ordered Pd. The work function of Pd evaporated from a W evaporator generally was usually appreciably lower (about 4.9 eV). The samples prepared by e-gun evaporation also exhibited sharper structure in the EDCs than did the samples prepared by evaporation from a W evaporator.

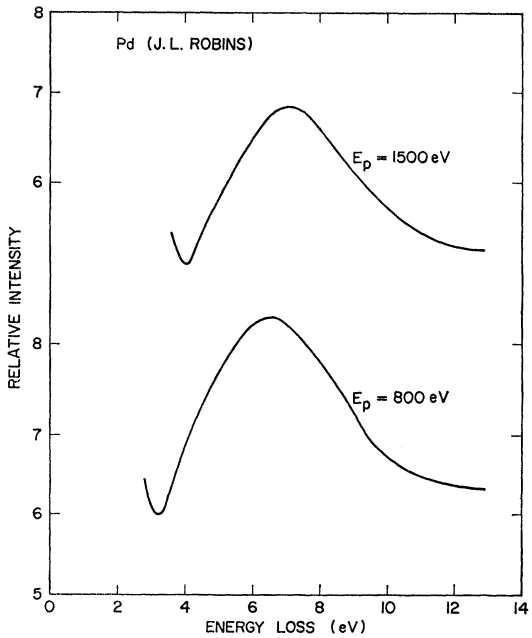

FIG. 8. Energy-loss spectrum of palladium with primary electron energy $E_p=800$ and 1500 eV from Robins (Ref. 13).

B. General Features of High-Vacuum Photoemitted Electron Energy Distribution Curves

If the EDCs have structure which superimpose on an $E-h\nu$ plot over a wide range of photon energies, the nondirect transition model is applicable and this structure is due to structure in the valence band.[3,5] If the EDCs are plotted versus $E-h\nu+\varphi$, to refer the energies to the states from which the electrons are excited the

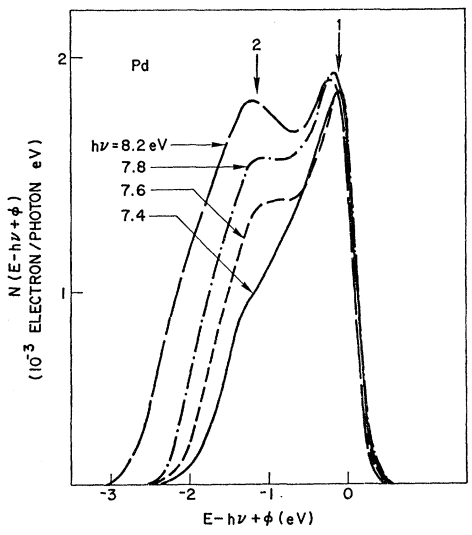

FIG. 10. Energy-distribution curves of palladium for $h\nu=7.4$–8.2 eV plotted versus $E-h\nu+\varphi$.

[14] R. H. Fowler, Phys. Rev. **38**, 45 (1931).
[15] R. Suhrmann and G. Wedler, Z. Angew. Phys. **14**, 70 (1962).

structure due to the valence band should superimpose for a large range of photon energy. In Figs. 10–12, we present EDCs which have been normalized to yield (NEDC) so that the area of each NEDC is equal to the quantum yield. In Figs. 10 and 11, the most pronounced characteristic feature is the superposition in the position of two of the peaks (under arrows 1 and 2) centered at $E-h\nu+\varphi=-0.1$ and -1.1 eV. For $h\nu>7.6$ eV, the NEDCs increase in height with photon energy $h\nu$. We shall come back to this point in Sec. VI. In Fig. 12, peaks 1 and 2 become obscured due to the effects of electron-electron scattering. A third peak (circled) starts to appear abruptly for $h\nu>9.8$ eV and is the strongest at $h\nu=10.8$ eV. It moves, but not with the exact increment of photon energies (see also Fig. 13). Because of the

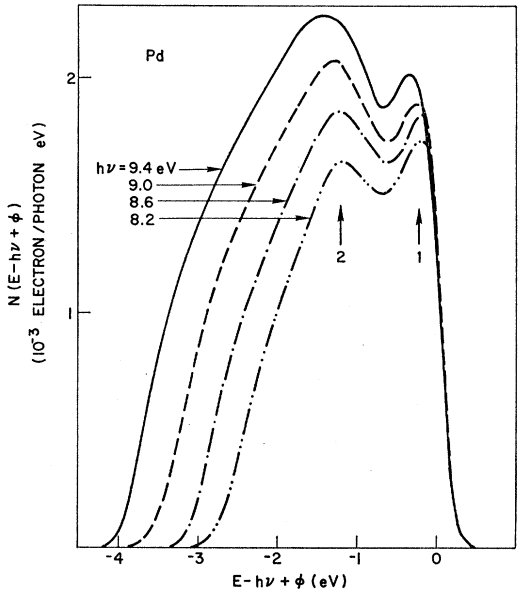

FIG. 11. Energy-distribution curves of palladium for $h\nu=8.2$–9.4 eV plotted versus $E-h\nu+\varphi$.

abrupt appearance of the peak and the manner in which it moves with $h\nu$, this piece of structure cannot be explained in terms of nondirect transitions with constant matrix elements. In fact, it has the characteristics that one would expect for a direct transition. It should be noted, however, that the strength of this transition is relatively weak, i.e., it provides perhaps 10–20% of the total oscillator strength. This will become more apparent when we compare, in Sec. VI, the NEDCs calculated on the nondirect model with those actually measured.

To summarize, two peaks in the EDCs, as well as an underlying continuum, are consistent with nondirect transitions. The peaks are due to valence-band states at $E-E_f=-0.1$ and -1.1 eV. A third piece of structure starts to appear for $h\nu>9.8$ eV which cannot be explained in terms of the nondirect-constant-matrix-

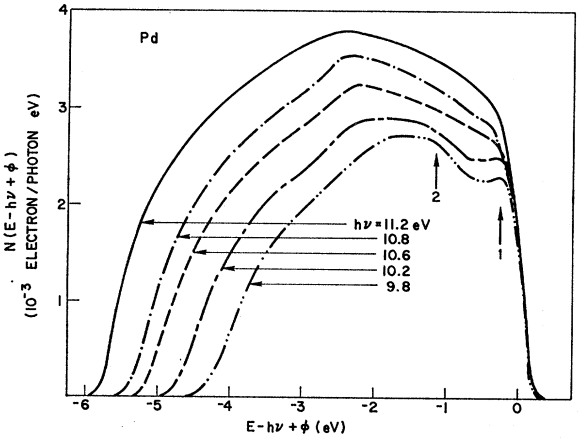

FIG. 12. Energy-distribution curves of palladium for $h\nu=9.8$–11.2 eV plotted versus $E-h\nu+\varphi$.

elements model. The heights of the EDCs increase with photon energy for $h\nu>7.6$ eV. This is an unusual effect which has not been observed previously in photoemission studies. Interestingly enough, $\omega\sigma$ also rises for $h\nu>7.6$ (Fig. 5). We shall discuss this point in more detail in Sec. VI.

C. Low-Vacuum Experiment for $h\nu>11.2$ eV

In Sec. II, a tube was described in which the LiF window could be knocked off in the 2×10^{-5}-Torr vacuum of the monochromator. In Fig. 14, EDCs are presented which were obtained for $h\nu=16.8$ and 21.3 eV. One 16.8-eV curve was completed 5 min after the window was knocked off; the second 16.8 eV was completed 5 min after the first. Since the gas in the arc had to be changed from neon to helium before the 21.3-eV curve could be taken, there was a longer time interval between the second 16.8- and the 21.3-eV measurements.

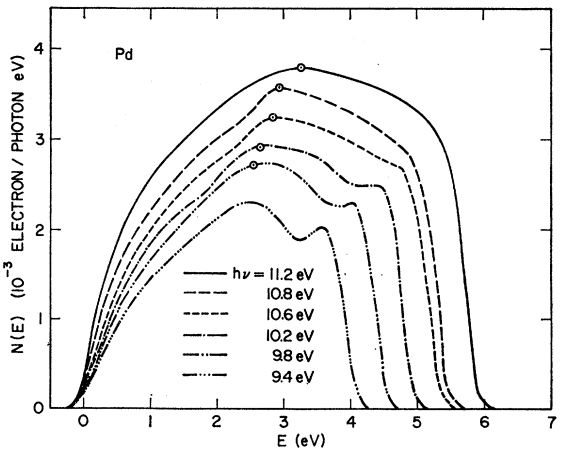

FIG. 13. Energy-distribution curves of palladium for $h\nu=9.4$–11.2 eV plotted versus E.

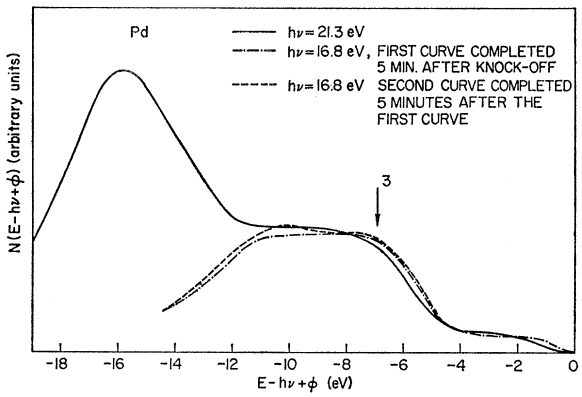

FIG. 14. Energy-distribution curves of palladium studied in poor vacuum for $h\nu=16.8$ and 21.3 eV plotted versus $E-h\nu+\varphi$.

In order to obtain some idea of the effect of the poorer vacuum on the EDCs, $h\nu=7.8$ eV curves were taken before the window was knocked off and after the completion of the 21.3-eV curve. These two curves are presented in Fig. 15. The EDC before knockoff is very similar to those obtained from the other heat-cleaned or e-gun evaporated samples (see Fig. 1). In comparing the high- and low-vacuum samples, it is clear that structure in the EDCs of the low-vacuum sample is very much smeared compared with those of the high-vacuum sample. Nevertheless, the structures (at $E=1$ and 2 eV) are still discernible. The fact that the structures were only broadened and smeared indicates that low-vacuum data could provide information about gross features, though not fine details.

From Fig. 14 it is clear that a piece of structure (labelled 3) is present at $E-h\nu+\phi\cong-7$ eV. This might be due to a peak in the valence-band optical density of states at $E-E_f=-7$ eV. However, because of the presence of large amounts of scattered electrons, the shape and height of this piece of structure cannot be unambiguously determined from this set of EDCs alone. This structure could also be due to electrons suffering plasmon loss since there are evidences of a strong plasmon resonance at about 7.5 eV. The origin of this structure will be discussed later. The large peak near

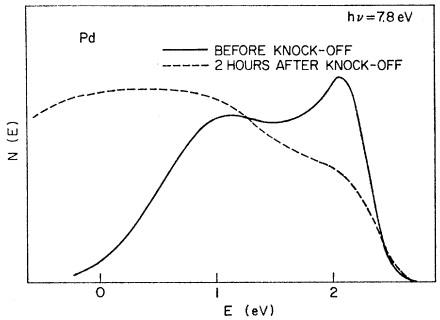

FIG. 15. Energy-distribution curves of palladium at $h\nu=7.8$ eV before and after exposure to monochromator vacuum.

-16 eV for $h\nu=21.3$ eV is probably due to electrons scattered by the ordinary electron-electron scattering event.[16]

V. ANALYSIS OF DATA

A. Determination of Optical Density of States

1. Introduction

In this section, we derive optical density of states (ODS) from the photoemission and optical data. In Sec. III, the relatively weak direct transition will be discussed. In the case of nondirect transitions, the NEDCs and optical conductivity are given by the expressions[17,18]

$$N(E,h\nu)=P(E)M^2N_V(E-h\nu)/\omega^2\sigma\,, \tag{1}$$

where

$$P(E)=\frac{\alpha L}{1+\alpha L}T(E)N_c(E)\,, \tag{2}$$

$$\omega\sigma(h\nu)=C\int_{Ef}^{E_f+h\nu}M^2N_c(E)N_V(E-h\nu)dE\,, \tag{3}$$

where M^2 is the momentum matrix element squared, α is the absorption coefficient, L is the characteristic length[17,18] for electron escape, and $T(E)$ is the probability of escape for an electron which reaches the surface with energy E.

From photoemission experiments, it is fairly easy to locate the position in energy of peaks in the ODS; it is somewhat more difficult to determine their relative magnitudes. As can be seen from Figs. 10–12, two strong peaks appear in the energy distributions due to excitation from initial states located at $E-E_f=-0.1$ and -1.1 eV. Thus, strong maxima in the ODS are located at these points. Since the -0.1-eV-peak structure appears near the maximum energy in the NEDCs, it is apparent that it cannot be due to electrons scattered from higher energies. It seems highly unlikely that the -1.1-eV peak can be due to scattered electrons since no strong 1.0-eV characteristic loss has been reported in Pd. The third major piece of structure is that near $E-E_f=-7$ eV, seen in the low-vacuum experiments (Fig. 14). When structure is located this far below the maximum energy, that data must be examined carefully to determine whether it is due to electrons scattered from higher energy, or to optical excitation from a peak in the ODS about 7 eV below the Fermi level. In the present case, the possibility that the peak is due to scattering is particularly strong since there appears to be strong plasmon loss of about 7.5 eV in Pd (see Figs. 7 and 8). It should be possible to determine

[16] W. E. Spicer, in *Optical Properties and Electronic Structure of Metals and Alloys* (North-Holland Publishing Co., Amsterdam, 1966), p. 296.

[17] C. N. Berglund and W. E. Spicer, Phys. Rev. **136**, A1030 (1966); **136**, A1044 (1964).

[18] W. F. Krolikowski, Ph.D. thesis, Stanford University, 1967 (unpublished).

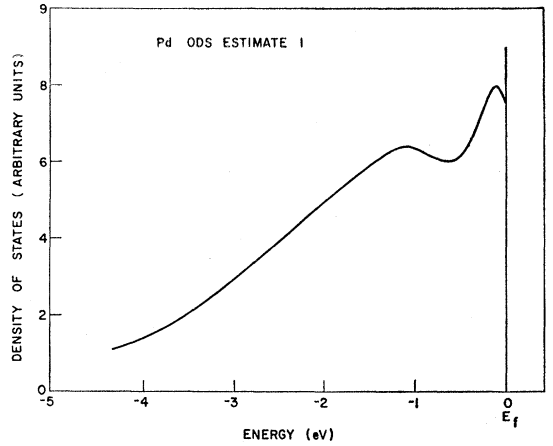

FIG. 16. The first estimate of the optical density of states of palladium below the Fermi surface.

whether the −7-eV peak is due to scattering or optical excitation, by requiring a self-consistent fit of the ODS to all of the available photoemission and optical data through the use of Eqs. (1)–(3).

Examination of the NEDCs of Figs. 10–12 shows a striking characteristic of the NEDCs for Pd. Whereas the NEDCs superimposes approximately for $h\nu<8.2$ eV, the NEDC rise on the absolute scale for $h\nu>8.2$ eV. This rise coincides with the rise in $\omega\sigma$ at about $h\nu>8$ eV.

2. *Calculation of NEDCs*

A. Model A. Figure 16 gives a first estimate of the optical density of states for $E_f-E>-4.4$. Using this, the escape function $P(E)=[(\alpha L/(1+\alpha L))T(E)N_c(E)]$ was determined from a few NEDC using Eq. (1), assuming M^2 is a constant. This is presented in Fig. 17. The zero of energy in Fig. 17 is set at the Fermi surface as in Fig. 16. A marked decrease in $P(E)$ for $E-E_f>7.5$ eV is obtained.

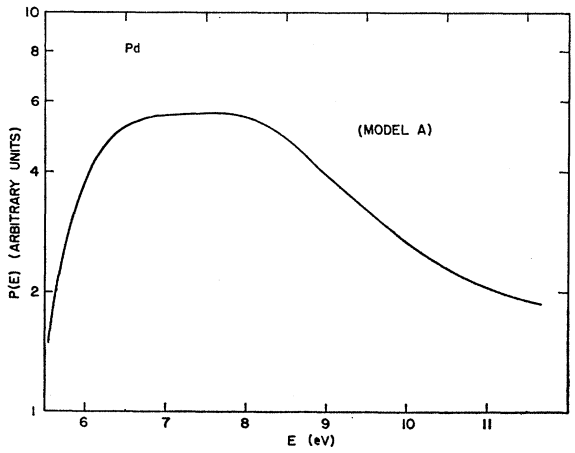

FIG. 17. The photoemission escape $P(E)$ of palladium based on model A.

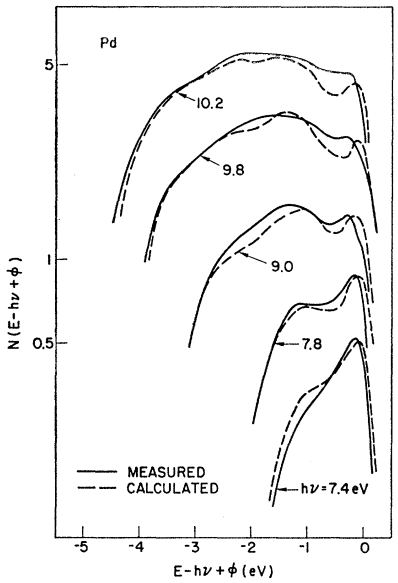

FIG. 18. Comparison of measured and calculated energy-distribution curves of palladium.

Once $N_V(E)$ and $P(E)$ have been determined for a few values of $h\nu$, they can be used to calculate NEDCs for the complete range of $h\nu$ studied. It was found that the shape of the experimental NEDCs could be fairly well reproduced by calculations using the $N_V(E)$ and $P(E)$ of Figs. 15 and 16, respectively. However, as might be expected from the NEDCs of Figs. 10–13, the absolute magnitude of the calculated NEDC could not be fitted to the experimental NEDC if the matrix element is assumed to be independent of $h\nu$. This is a reflection of the monotonic increase of the magnitude of the NEDCs for *all* values of electron energy with increasing $h\nu$ (see Figs. 10–13) for $h\nu>7.6$ eV. In order to fit the magnitude of the NEDCs, it was necessary to assume that the square of the matrix element for 11.6 eV $>h\nu>7.6$ eV is given by $M^2(h\nu)=\text{const}\times e^{\beta(h\nu-7.6)}$, where $\beta=0.688$/eV. Using the $h\nu$-dependent matrix element and the $N_V(E)$ and $P(E)$ of Figs. 16 and 17, the absolute fits between calculated and measured NEDC shown in Fig. 18 were obtained.

It should be emphasized that a monotonic increase of matrix element with increasing $h\nu$ for transition of all final energy states cannot be explained in terms of direct transitions. It is interesting to note that the onset of the matrix element increase occurs quite near the plasma energy.[19]

In order to calculate $\omega\sigma$, we must have values for the ODS from the Fermi level to 12 eV above the Fermi level and to the bottom of the valence band. In Fig. 19, we give an ODS extending over the indicated energy range. Using this ODS, Eq. (3), and the matrix element squared (consistent with the findings in Sec. IV) indi-

[19] R. K. Nesbet and P. M. Grant, Phys. Rev. Letters **19**, 222 (1967); and private communication.

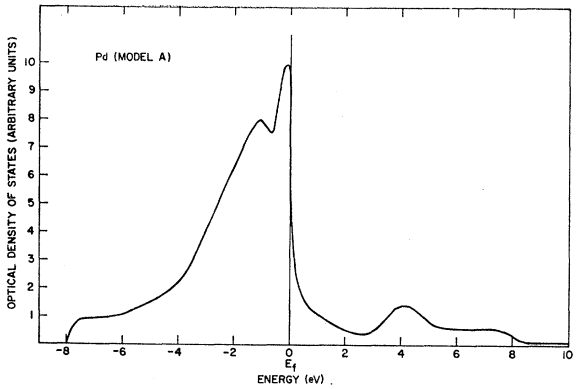

FIG. 19. Optical density of states of palladium, model A.

cated below:

$$M^2(h\nu)=A, \quad \text{for } 0<h\nu<7.6 \text{ eV} \quad (4)$$
$$M^2(h\nu)=Ae^{\beta(h\nu-7.6)}, \quad \text{for } h\nu>7.6 \text{ eV}$$

the $\omega\sigma$ curve indicated in Fig. 20 was calculated. As can be seen, good agreement is obtained between the calculated and measured $\omega\sigma$. Since the absolute magnitude of the matrix elements cannot be calculated, the calculated $\omega\sigma$ was fitted to the experimental $\omega\sigma$ for one value of $h\nu$.

The lowest-energy peak in $\omega\sigma$ (near $h\nu=2$ eV) is seen to be due to coupling of the high-filled density of states within 2 eV of the Fermi surface to the empty density of states within 1 or 2 eV of the Fermi surface. The strong shoulder in $\omega\sigma$ above about 4 eV is due to coupling of the high density of valence states within 2 eV of the Fermi surface and the peak in the conduction density of states centered at about 4 eV. The monotonic rise in $\omega\sigma$ from 7.6 to 11.6 eV is due to the increase of the matrix element with $h\nu$. It should be noted that good agreement is obtained between the measured and the calculated $\omega\sigma$ without placing a peak in the ODS near 7.5 eV. Thus, it appears that the structure seen in the EDCs at about 7.5 eV below the maximum energy for $h\nu=16.8$ and 21.3 eV (see Fig. 14) is due to scattering via the strong plasma peak at 7.5 eV. (See Figs. 7 and 8.)

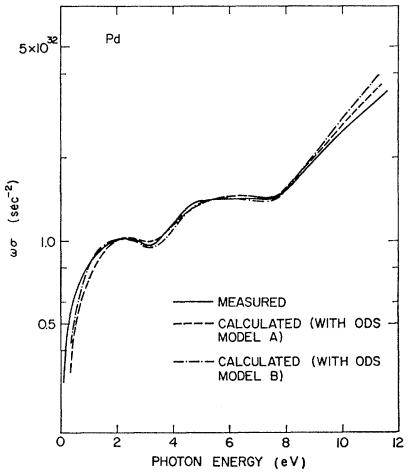

FIG. 20. Comparison of measured and calculated $\omega\sigma$ calculated on the basis of models A and B. The calculated curves have been fitted to the experimental curve at 6 eV.

B. Model B. If the matrix element is not a constant and if there is no independent means of determining $P(E)$, there is a certain lack of uniqueness in the ODS. In particular, the same calculated NEDC and $\omega\sigma$ values would be obtained if part of the exponential dependence in the matrix element was transferred to the valence-band ODS and $P(E)$ adjusted accordingly. Thus we can write

$$M^2=A, \quad \text{for } 0\leq h\nu\leq 7.6 \text{ eV} \quad (5)$$
$$M^2=Ae^{\beta_1(h\nu-7.6)}, \quad \text{for } h\nu>7.6 \text{ eV} \quad (6)$$
$$N_V'(E)=N_V(E)e^{-\beta_2(E)}, \quad (7)$$
$$P'(E)=P(E)e^{\beta_2(E)}, \quad (8)$$

where

$$\beta_1+\beta_2=\beta.$$

Of course, the way β is divided is completely arbitrary as long as the resultant ODS is everywhere positive and consistent with the photoemission and optical-reflectivity data. If we let $\beta_1=0$, the resultant ODS is not physical, since agreement can only be obtained with $\omega\sigma$ if $N_c(E)$ is negative for certain values of energy. However, if we divide β into two almost equal parts, $\beta_1=0.388$ (eV)$^{-1}$ and $\beta_2=0.3$ (eV)$^{-1}$, the calculated $\omega\sigma$ is in good agreement with the experiment (Fig. 20), provided that the ODS shown in Fig. 21 is used. A fit with the NEDC is also preserved if $P(E)$ takes the form shown in Fig. 22. Note that N_V and $P(E)$ shown in Figs. 21 and 22 were obtained from N_V and $P(E)$ in Figs. 13 and 17 by Eqs. (7) and (8), respectively. The features of the ODS are similar to the previous estimates except that the relative heights of the two peaks in the valence band are modified and a sharp decrease in the conduction-band density of states

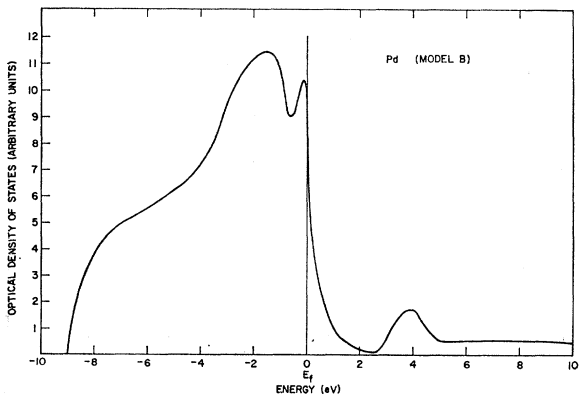

FIG. 21. Optical density of states of palladium, model B.

$N_c(E)$ is not obtained near 8 eV. Note also that $P(E)$ does not drop strongly for $E>8.0$ eV. The rate of increase of matrix element with $h\nu$ is considerably less than that for model A. In the Appendix, we present an example of data on the electron-electron scattering length. The authors believe that model B is probably better than model A since model B leads to density of states above the Fermi level which is simpler than model A and because it requires a less rapidly increasing matrix element for $h\nu>7.6$ eV.

3. *ODS Obtained from Models A and B*

Due principally to the increase of matrix element for $h\nu>7.6$ eV, it is somewhat more difficult to determine the magnitude of the ODS than in the study of other transition and noble metals at a given energy; however, it should be emphasized that the location of structure in the ODS is not affected by this. This uncertainty is reflected in the difference between the ODS of Figs. 19 and 21.

By associating 10 electrons/atom with the states below the Fermi energy, it is possible to obtain an estimate of the density of states at the Fermi level. Because of the rapid rise of the density of states near the Fermi energy, the uncertainty in this estimate is probably at least $\pm 50\%$.

Values of 3.1 and 1.4 electron/atom eV were obtained for the density of states of models A and B, respectively. These results can be compared with those obtained from band calculations. Freeman, Dimmock, and Furdyna[20] obtained a density of states at the Fermi level of 1.76 electron/atom eV, whereas, in a recent relativistic calculation, Andersen and Mackintosh[21] obtained a value of 2.35 electron/atom eV.

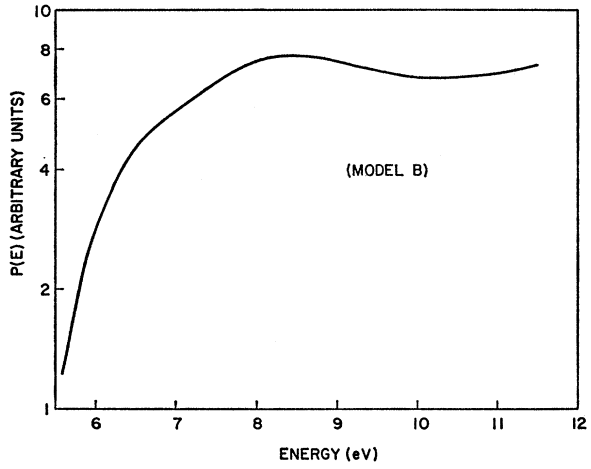

FIG. 22. The photoemission escape $P(E)$ of palladium based on model B.

[20] A. J. Freeman, J. O. Dimmock, and A. M. Furdyna, J. Appl. Phys. **37**, 1256 (1966); and private communication.
[21] O. K. Andersen and A. R. Mackintosh (private communication).

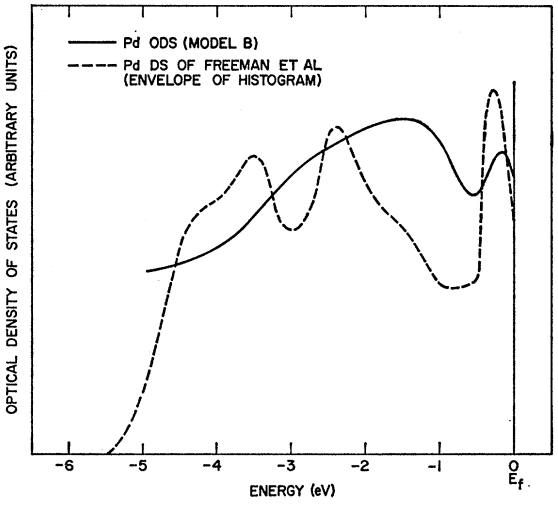

FIG. 23. Comparison of palladium optical density of states (model B) with the calculated density of states of Freeman *et al.* (envelope of their histogram), Ref. 20.

The density of states at the Fermi energy obtained in this work can also be compared with the density of states obtained from specific-heat measurements of 3.96 electrons/atom eV.[22] The electron-phonon interaction and spin fluctuations[23] will increase the specific-heat density of states above the band or bare density of states, whereas these effects mechanisms should not affect the results obtained from the photoemission and optical experiments because of the "sudden" nature of an optical transition.

Values between 0.5 and 0.7 holes/atom are obtained from the ODS curve. These should be compared with the values of 0.58, 0.36, and 0.375 holes/atom obtained, respectively, from specific-heat[22,24] de Hass–van Alphen[25] measurements, and band[21] calculations, respectively.

In Fig. 23, we compare the ODS obtained in this work with that calculated by Freeman *et al.*[20] for $-5.5\leq E-E_f\leq 0$. Note that in this work we find the bottom of the band to be approximately 8 eV below the Fermi level compared with 5.5-eV depth found by Freeman *et al.* In both the ODS and the calculation density of states, a high density of states is found just below the Fermi level; however, we find only one broad peak at lower energies, whereas the calculation gives two sharper peaks somewhat lower than our single broad peak.

In previous photoemission studies it was found that the ODS of Cu and Ni were not closely related by the rigid-band model. In Fig. 24, a comparison is made

[22] M. Shimizu, T. Takahashi, and A. Katsuki, J. Phys. Soc. Japan **18**, 240 (1963).
[23] N. F. Berk and J. R. Schrieffer, Phys. Rev. Letters **17**, 433 (1966); S. Doniach and S. Englesberg, *ibid.* **17**, 750 (1966).
[24] N. K. Hindley and P. Rhodes, Proc. Phys. Soc. (London) **81**, 717 (1963).
[25] J. J. Vuillemin, Phys. Rev. **144**, 396 (1966).

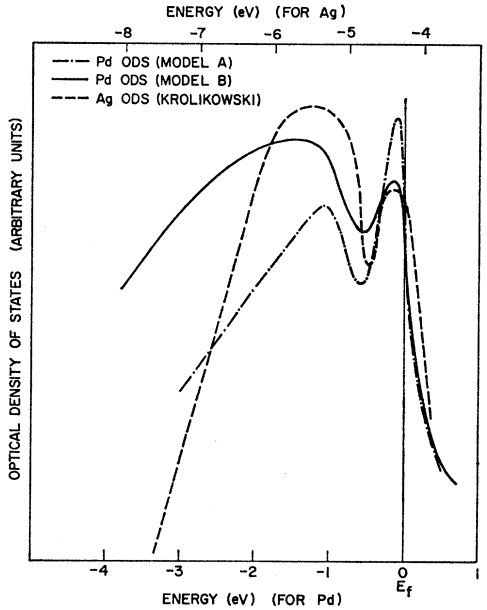

FIG. 24. Comparison of the optical density of states of palladium and silver. The silver optical density of states has been shifted in energy so that the first strong peak is aligned with that of palladium.

between the d-band ODS obtained from Pd and Ag. (The Ag results are from the recent work of Krolikowski,[18] and they are almost identical with the earlier work of Berglund and Spicer.[17]) As can be seen from Fig. 24, the two strong peaks in the ODS coincide quite nicely, thus indicating that they are closely related via the rigid-band model. A principal difference between the ODSs for Ag and Pd is that the d bands appear to be appreciably wider in Pd than in Ag. However, part of the Pd width may be due to the effect of s and/or p states lying below the d states and/or to the hybridization of these states with d states. It is also interesting to note that density-of-states peaks were found about 3.5 eV above the top of the d band in both Ag and Pd.

B. Direct Transitions

As mentioned previously, the broad peak which appears in the NEDCs for $h\nu \geq 9.0$ eV (see Figs. 12 and 13) moves to higher energy with increasing photon energy by an amount less than the increase in photon energy, i.e., it moves in a manner expected for a direct transition. Thus this appears to be the first observation in photoemission of direct transitions from the region of the d bands or a noble or transition metal. It might be associated with s and/or p states near the bottom of the d band. These states will, of course, be hybridized with the d states. It is interesting to note that in nonferromagnetic Pd this direct transition is found, whereas in the ferromagnetic metals lying at the end of the first transition series no direct transition is observed from the d band, but a very strong peak is observed in the EDCs due to nondirect transitions from a peak in the ODS about 5 eV below the Fermi surface.

VI. COMPARISON WITH NICKEL AND OTHER FERRO- AND ANTIFERROMAGNETIC TRANSITION METALS

As stated in the Introduction, a principal motivation of this work was the comparison of Pd with the ferromagnetic transition metals lying just above it in the periodic table. In Fig. 25, we present the ODS of states of Fe,[1] Co,[2] Ni,[3] and Cr.[4] These should be compared with the ODS for Pd obtained for the two models, presented in Fig. 25(b). The striking difference between these two sets of ODS is the presence of the deep peak at about -5 eV in the ferro- and antiferromagnetic materials and the absence of these peaks in Pd, which is paramagnetic. In order to make it completely clear that the appearance of this peak is not an artifact of the data analysis, i.e., of obtaining the ODS from the NEDCs, we present in Fig. 26 the NEDCs for Ni, Co, and Pd for $h\nu = 10.2$ eV. As can be seen, the deep peak is present in the ferromagnetic material but not in the paramagnetic material. Figure 26 is presented to emphasize the fact that the appearance of the deep peak in the ODS does not depend on the details of analysis but on the presence or absence of this peak in the raw experimental data.

VII. CONCLUSIONS

In Sec. VI, Figs. 25(a) and 25(b), we compared the ODS of Pd with those of the Ni and the other ferromagnetic transition metals Co and Fe as well as the antiferromagnetic Cr. Strikingly, there is no evidence for the

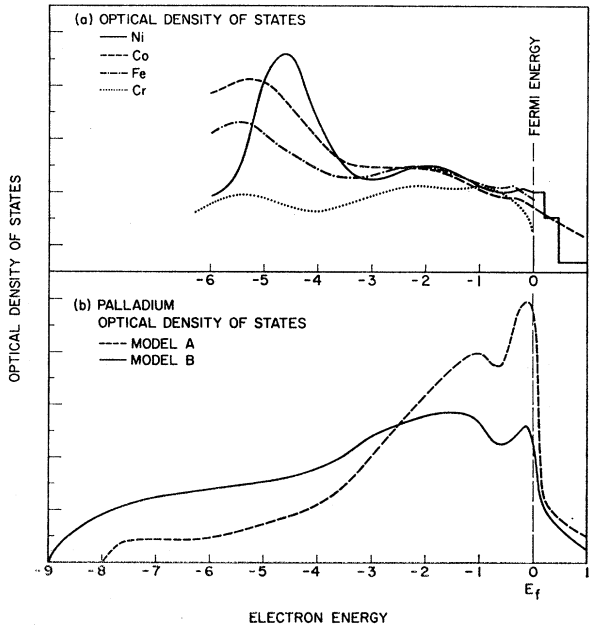

FIG. 25. Comparison between the optical density of states of four members of the first transition-metal series and palladium.

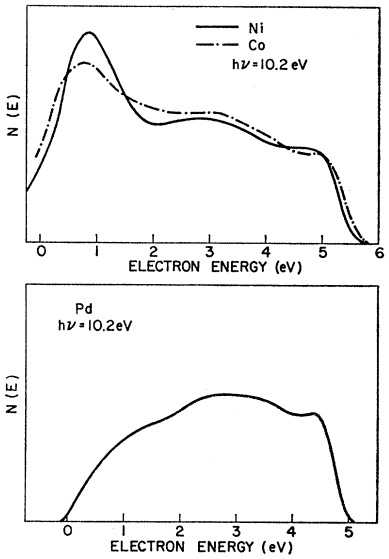

FIG. 26. Comparison of the energy-distribution curves at $h\nu=10.2$ eV of Ni, Co, and Pd. Note that a peak appears near the zero of energy for Ni and Co but not for Pd.

strong peak which appears in the ODS of Ni, Co, Fe, and Cr at about 5 eV below the Fermi level. In a previous paper on Co,[2] there was a detailed discussion of some of the possible implications of the 5-eV peak, which will not be repeated here. However, we will reemphasize the importance of comparing the ODS obtained from related materials. The appearance of the 5-eV peak in Ni, Co, Fe, and Cr, but not in Pd, indicates the presence of strong interactions in the former metals which are not present in Pd. Although the appearance of these interactions correlates with the occurrence of ferro- or antiferromagnetism, additional study will be necessary in order to determine whether or not this correlation is accidental or meaningful.

Another point of interest is the applicability or lack of applicability of the rigid-band model. For the last members of the first transition series (Fe, Co, Ni, and Cu), it appears impossible to relate the ODS using the rigid-band model. In contrast, the principal structure in Pd and Ag (at the end of the second transition-metal series) are well related via the rigid-band model.

From these measurements it is possible to obtain an estimate of the density of states at the Fermi level. Because of the sudden nature of an optical transition, one would expect that the ODS is not to be affected by the electron-phonon interactions or spin fluctuations[23] which are important in electronic specific-heat measurements; however, the accuracy in the present work is not high. For the two models used in the analysis of the photoemission and optical data, values of 3.1 and 1.4 electrons/atoms eV were obtained for the density of states at the Fermi energy. These values are to be compared with values of 1.76 and 2.35 states/atom eV obtained from band calculations[20,21] and with the value of 3.96 electrons/atom eV obtained from electronic specific-heat measurements.[22] The present results lie somewhat lower than the results from the specific-heat measurements, as is to be expected since the density of states obtained from those measurements will be enhanced by electron-phonon or magnetic interactions. The results from the band calculation lie within the range of values obtained in this work.

ACKNOWLEDGMENTS

The authors are grateful to Dr. A. Freeman, Dr. R. Nesbet, and Dr. P. Grant for helpful discussions.

APPENDIX: ESTIMATE OF $L(E)$, THE ELECTRON ESCAPE LENGTH

After determining $P(E)$ (Fig. 22), we can solve for $L(E)$ from Eq. (2);

$$L(E)=-\frac{1}{\alpha N_c(E)T(E)-P(E)}\frac{P(E)}{}. \tag{9}$$

Though we do not have an independent method of measuring $T(E)$, a simple free-electron form of $T(E)$ [17] will be assumed in our estimates of $L(E)$.

$$T(E)=\tfrac{1}{2}\{1-[(\varphi-E_\beta)/(E-E_\beta)]^{1/2}\} \text{ if } E\geq\varphi$$
$$=0 \text{ if } E<\varphi. \tag{10}$$

In this equation, the Fermi level is taken to be the zero of energy and E_β is an adjustable parameter. Two values of E_β have been chosen: 3.6 and 4.0 eV, and the two resultant $L(E)$ curves are shown in Fig. 27. Also shown is the calculated electron-electron scattering length $1_e(E)$ leased on the free-electron model,[18] normalized at $E-E_f=1$ eV to the data of Sze *et al.*[26] It is seen that the agreement between $L(E)$ obtained from photoemission data and $1_e(E)$ of free-electron model is reasonable. The shoulder appearing at about 8 eV of $L(E)$ is possibly due to the fast decrease in N_V to zero near $E-E_f=-8$ eV.

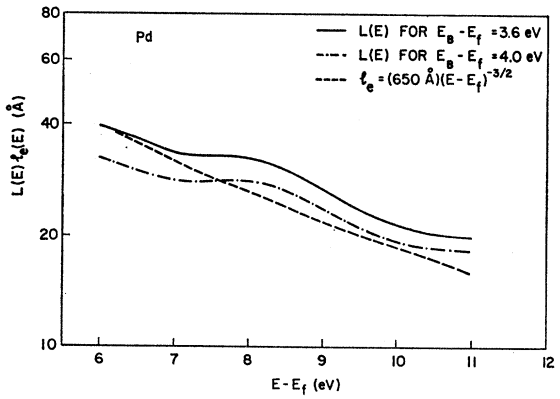

FIG. 27. Comparison of calculated $l_e(E)$ with $L(E)$ deduced from photoemission data. The calculation is based on a free-electron model with the bottom of the conduction band E_B placed as indicated in the figure.

[26] S. M. Sze, C. R. Crowell, J. G. P. Carey, and E. E. LaBate, J. Appl. Phys. 37, 2690 (1966).